Available online at www.sciencedirect.com
ScienceDirect
Acta Materialia 59 (2011) 5544–5557
Acta MATERIALIA
www.elsevier.com/locate/actamat

Modeling grain size dependent optimal twin spacing for achieving ultimate high strength and related high ductility in nanotwinned metals

Linli Zhu [a], Haihui Ruan [a], Xiaoyan Li [b], Ming Dao [c], Huajian Gao [b], Jian Lu [d,*]

[a] Department of Mechanical Engineering, The Hong Kong Polytechnic University, Hung Kom, Kowloon, Hong Kong, China
[b] School of Engineering, Brown University, 182 Hope Street, Providence, RI 02912, USA
[c] Department of Materials Science and Engineering, Massachusetts Institute of Technology, 77 Massachusetts Avenue, Cambridge, MA 02139, USA
[d] Department of Manufacturing Engineering and Engineering Management, City University of Hong Kong, Hong Kong, China

Received 29 March 2011; received in revised form 10 May 2011; accepted 12 May 2011
Available online 12 June 2011

Abstract

We have developed a mechanism-based plasticity model of nanotwinned metals to investigate the effect of twin spacing on strength, ductility and work hardening rate of such materials. In particular, the unique roles of dislocation pile-up zones near twin and grain boundaries, as well as twinning partial dislocations, in strengthening and work hardening are incorporated in the model. Competition between different local failure mechanisms associated with twin lamellae and/or grain boundaries is considered in evaluating the tensile ductility of nanotwinned metals. The present study provides a quantitative continuum plasticity model capable of describing the variations in strength, ductility and work hardening rate of nanotwinned metals with the twin spacing. For nanotwinned copper a grain size of 500 nm, the model predicts a critical twin spacing for the maximum strength at 13 nm, in excellent agreement with experimental observations. The critical twin spacing is found to be linearly proportional to the grain size, which is consistent with recent molecular dynamics simulations.
© 2011 Acta Materialia Inc. Published by Elsevier Ltd. All rights reserved.

Keywords: Nanotwinned metal; Strength; Ductility; Density of dislocations; Dislocation pile-up zone

1. Introduction

High strength and high ductility are becoming increasingly desirable for the metals and alloys that are widely used in modern technologies. This key issue has stimulated widespread interest in the materials community [1]. Recent decades have seen the emergence of several strategies for producing materials of ever-greater strength, such as grain size refinement, solid solution alloying and plastic straining. Unfortunately, most of the existing material-strengthening techniques result in decreased ductility [2,3]. This strength–ductility trade-off can be circumvented by several alternative approaches that involve sophisticated microstructure design, including metals with bimodal grain sizes [4,5], composites with an amorphous phase and nanograins [6], as well as laminated materials [7]. More recently, engineering coherent internal boundaries at the nanoscale has been regarded as an efficient way to achieve high strength while maintaining substantial ductility [2,8,9]. Tensile tests of nanotwinned copper [10] revealed the maximum yield strength at a critical twin spacing around 15 nm. Below this value, both ductility and strain hardening rate were seen to increase with further reduction in twin spacing. It is thus important to determine this critical twin spacing and how it varies with other material parameters, in order to produce materials with optimal properties.

Although twin boundaries (TBs) often strengthen the material in a similar way to grain boundaries (GBs), there exists a fundamental difference between TBs and GBs in affecting the plastic deformation. As the grain size is on the order of hundreds of nanometers in nanotwinned cop-

* Corresponding author. Tel.: +852 3442 9811; fax: +852 34420295.
E-mail address: jianlu@cityu.edu.hk (J. Lu).

1359-6454/$36.00 © 2011 Acta Materialia Inc. Published by Elsevier Ltd. All rights reserved.
doi:10.1016/j.actamat.2011.05.027

per, intragrain dislocation-mediated plasticity is still important for most of the available deformation mechanisms. Dislocation–TB interactions, which have been confirmed by atomistic simulations, are considered to be the underlying mechanism for strengthening, strain hardening and toughening in nanotwinned copper [11,12]. Lattice dislocations are usually nucleated from free surfaces or grain boundaries, and TBs could act as additional dislocation sources under further plastic deformation [13–15]. The increase in yield stress in nanotwinned copper is mainly induced by the pinning effects of TBs on dislocations (e.g. the Lomer–Cottrell locking) [16,17]. The TBs could also result in an increase in strain hardening [18]. Zhu et al. [19] showed through atomistic simulations that the high ductility of nanotwinned copper might be attributed to a gradual loss of coherence of TBs during deformation.

Based on the atomistic simulations and experimental observations, two- and three-dimensional crystal plasticity models for nanotwinned ultrafine polycrystalline copper were established by introducing the concept of a twin-boundary affected zone (TBAZ) [20,21]. These continuum models account for the fact that TBs result in strong plastic anisotropy and rate-sensitivity anisotropy. A failure criterion was also proposed in these studies to quantitatively estimate the tensile ductility, leading to simulation results capable of capturing the macroscopic tensile strain–stress behavior as well as the increase in strength, rate-sensitivity and ductility with the reduction in twin spacing [20,21]. In other studies, models for twinning-induced plasticity steel were proposed to investigate the associated strain hardening mechanisms [22–24]. These models describe the dependence of isotropic or kinematic hardening on the size of microstructures in steels, including grain size and twin spacing.

In spite of the intensive research activity and rapid progress in this field, none of the existing theoretical models can predict the existence of the optimal twin spacing observed in experiments with nanotwinned copper. On other words, a physics-based constitutive model that can accurately describe the relationship between the microstructures and macroscopic mechanical properties of nanotwinned metals is still lacking. In the present work, we seek to develop a mechanism-based plasticity model of nanotwinned metals to account for the variation in strength, ductility and work hardening rate in these materials by incorporating the competition and transition of different deformation mechanisms as the twin spacing is reduced. The proposed approach invokes the concept of a dislocation pile-up zone near TBs and incorporates the unique roles of twinning partial dislocations in the constitutive model. Experiments have shown that the crystal lattice is elastically strained near TBs or GBs during plastic deformation, leading to piling up/accumulations of dislocations near these boundaries [20,25]. From this perspective, we postulate that strong local strain gradients may exist within the twin boundary dislocation pile-up zone (TBDPZ) and the grain boundary dislocation pile-up zone (GBDPZ). In the following, we will briefly review the main experimental findings/observations on nanotwinned copper before elaborating on our theoretical model and associated numerical results and discussions.

2. Experimental observations

By means of pulsed electrodeposition, Lu and coworkers [10,26,27] synthesized copper samples with nanoscale twins spaced from 4 to 96 nm embedded in submicron grains 400–600 nm in size, and reported two distinct mechanical behaviors of such nanotwinned copper with respect to the twin spacing. The first behavior is that the yield strength of the nanotwinned copper reaches a maximum, corresponding to a strengthening/softening transition, at a critical twin spacing of 15 nm, as shown in Fig. 1. The second is that the ductility of the nanotwinned copper increases monotonically with decreasing twin spacing. Pronounced increases in ductility and strain hardening rate occur when the twin spacing is smaller than 15 nm. It has been proposed that, at larger twin spacing, the strength of such nanotwinned copper is dominated by the TBs' resistance to dislocation activities. As the twin spacing is reduced to less than 15 nm, nucleation of twinning partial dislocations at TB–GB intersections could lead to a reduction in yield strength [28]. The activities of twinning partial dislocations start to dominate the plastic deformation with further reduction in twin spacing and lead to more pronounced strain hardening.

Recently, in situ tensile tests conducted under a transmission electron microscope have provided valuable observations for the transition of deformation and fracture mechanisms in nanotwinned copper [29]. These observations demonstrated that the crack edges follow a specific crystallographic direction at relatively large twin spacings (e.g. greater than 30 nm), while at relatively small twin spacings the crack morphology exhibits fewer crystallographic characteristics. This disparity of failure

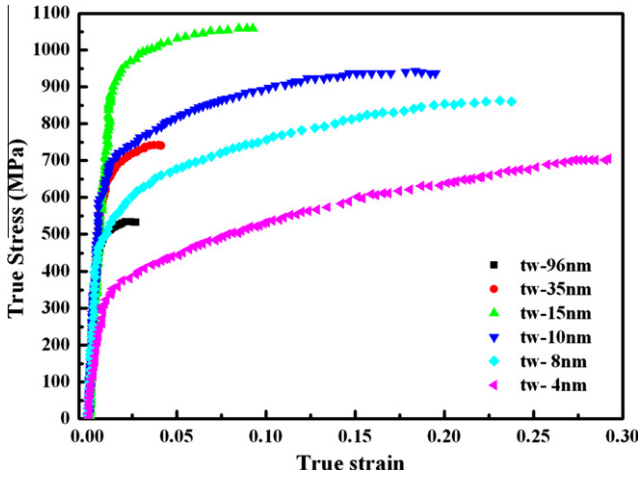

Fig. 1. Tensile stress–strain curves for as-deposited nanotwinned copper samples with mean twin thickness varying from 96 to 4 nm [10].

mechanisms suggests a transition in the plastic deformation mechanism from one dominated by dislocations inclined to the TBs in the case of large twin spacing to one dominated by twinning partial dislocation in the case of small twin spacing. Motivated by these experimental observations, a mechanism-based plasticity model that accounts for special dislocation activities near TBs and GBs, and involves the transition of different deformation mechanisms, is developed below. This model will be guided by, and aims to describe, the experimentally observed mechanical behaviors of nanotwinned copper.

3. Theoretical model

3.1. Flow stress in nanotwinned metal

A critical assumption of our theoretical model is the existence of a TBDPZ near TBs and a GBDPZ near GBs (see Fig. 2a). The effective thickness of the TBDPZ and GBDPZ is assumed to range from 7 to 10 lattice parameters [20,25]. Due to the critical importance of this assumption, we conducted a large number of parallel molecular dynamics (MD) simulations of dislocations interacting with a TB in nanotwinned copper to validate the existence of the TBDPZ, as shown in Fig. 3. In the simulation, a pre-existing crack is used as a "dislocation gun" that emits hundreds of dislocations which impinge on the TB.[1] The simulation verified the existence of a dislocation pile-up zone 5–7 nm in thickness around the TB, in excellent agreement with experimental observations [20]. In the TBDPZ, the dislocation density is much higher than elsewhere. For sufficiently small twin spacing, experiments have shown that few dislocations are stored inside the twin lamellae. Thus, the variation in dislocation density is a key parameter for the modeling of nanotwinned metal. Letting ρ_{TB}, ρ_{GB} and ρ_I denote the dislocation densities in the TBDPZ, the GBDPZ and the crystal interior, respectively, we have the following Taylor-type relationship between the flow stress and dislocation density:

$$\sigma_{flow} = \sigma_0 + M\alpha\mu b\sqrt{\rho} + \sigma_b \tag{1}$$

where $\rho = \rho_I + \rho_{TB} + \rho_{GB}$ is the total density of dislocations; α, μ and M are the Taylor constant, the shear modulus and the Taylor factor, respectively; σ_0 is the lattice friction stress and σ_b denotes the back stress that induces kinematic hardening (discussed further below). It should be noted that there is significant plastic anisotropy for a crystal with nanotwins. In principle, the local anisotropy among different grains can be incorporated into the Taylor factor M in the flow stress expression. However, for simplicity, we assume that the plastic deformation of nanotwinned metals can be represented by an averaged Taylor factor. In this sense, a unit cell of nanotwinned metal is adopted to investigate the deformation behavior of a polycrystalline sample with randomly oriented grains/twins, as shown in Fig. 2a.

Owing to large variations in dislocation density from one TB/GB to another, the equivalent shear strain can also vary significantly, leading to notable strain gradients in the TBDPZ and GBDPZ [20]. We thus postulate that the densities of dislocations in the TBDPZ and GBDPZ are functions of the corresponding strain gradients. The strain in the interior region of a crystal is presumably uniform. Atomistic simulations have revealed that the deformation of nanotwinned copper below the critical twin spacing is dominated by the nucleation and propagation of highly organized partial dislocations parallel to the TBs, the so-called twinning partial dislocations or twinning partials [28]. For materials with twin spacing above the critical value, the deformation is typically dominated by dislocations inclined to the TBs, following the traditional Hall–Petch relationship, in which case the density of twinning partial dislocations can be safely ignored. With the decrease in twin spacing down to less than the critical value, such as 15 nm for nanotwinned copper, the density of twinning partial dislocations increases so sharply that their contribution to the flow stress and work hardening must be taken into account. In the following, we consider the variation in dislocation density in different zones in a nanotwinned crystal.

3.1.1. Evolution of dislocation density in TBDPZ

Since the TBDPZ refers to the region adjoining the TBs where the crystalline lattice is elastically strained due to the pile-up of dislocations during plastic deformation, we assume that the plastic strain in the TBDPZ originates from dislocations stored in this region. As shown schematically in Fig. 2b, the shear strain caused by dislocations in the TBDPZ can be written as

$$\gamma_F^{TB} = \frac{\phi_1 n_F^{TB} \cdot b}{d_G} \tag{2}$$

where n_F^{TB} is the number of inclined dislocations around the twin boundaries and d_G is the size of a unit cell considered to be the grain size, as shown in Fig. 2a; ϕ_1 is a geometrical factor for the twin lamellae and b is the magnitude of the Burgers vector. It has been revealed by atomistic simulations that the activity of twinning partial dislocations in the twin lamellae becomes dominant when the twin lamellae spacing falls below the critical size. These dislocations will also contribute to the shear strain in the TBDPZ, which can be expressed as

$$\gamma_P^{TB} = \frac{\phi_2 n_P^{TB} \cdot b/\sqrt{3}}{d_G} \tag{3}$$

Here, n_P^{TB} is the number of twinning partial dislocations in the TBDPZ and ϕ_2 is the geometric factor. The total shear strain stemming from dislocations in the TBDPZ can thus be represented as

[1] A similar set-up has also been adopted in molecular dynamics simulations of crack interactions with TBs in free-standing copper thin films [30].

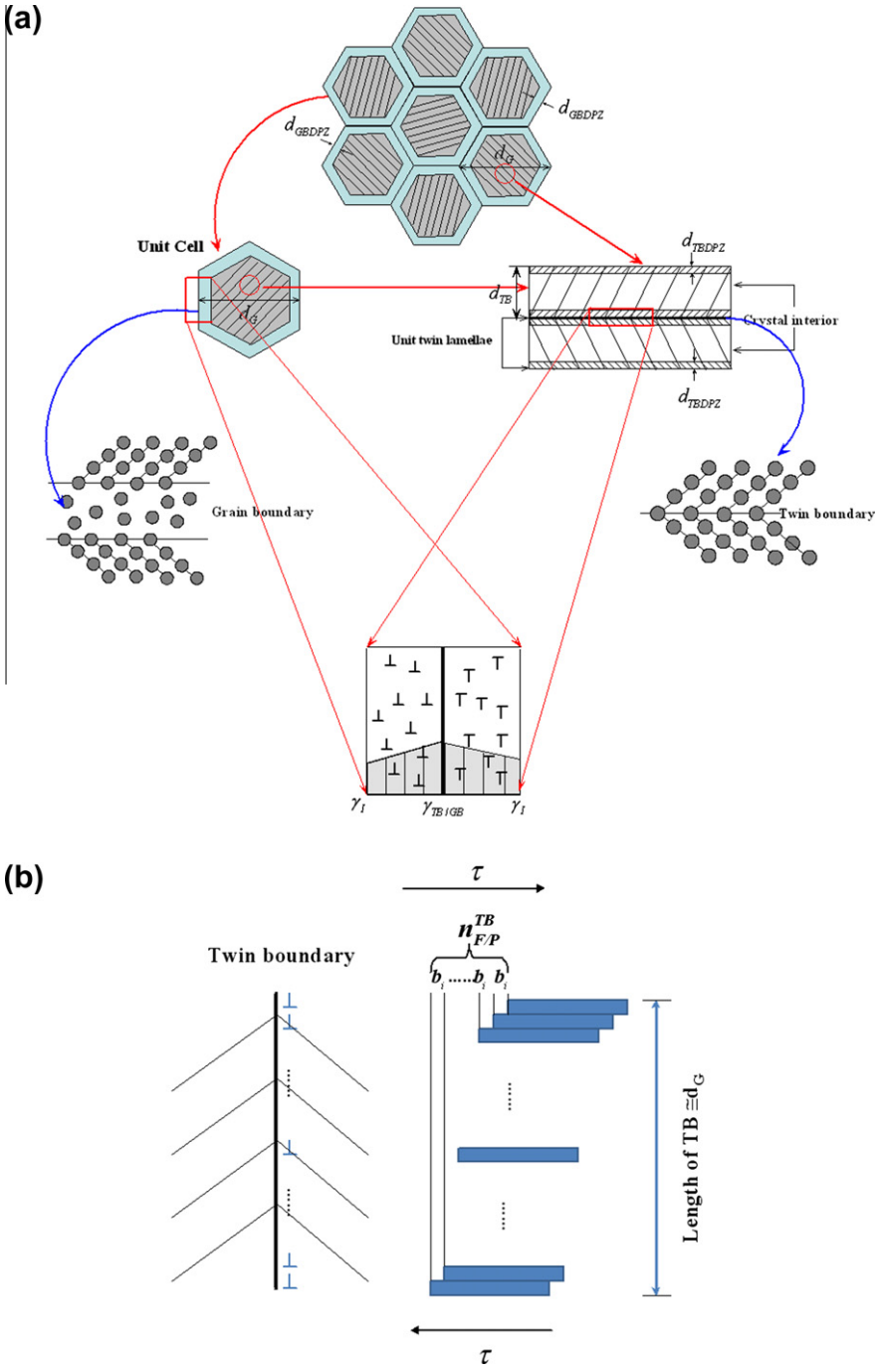

Fig. 2. (a) Schematic drawings of the proposed model for nanotwinned polycrystalline metal in which the TBDPZ and GBDPZ are introduced. (b) A schematic illustration of shear strain originated from dislocation accumulations in the TBDPZ in which $\mathbf{b}_i (i = \mathbf{F}, \mathbf{P})$ is the magnitude of the Burgers vector for full dislocation and/or partial dislocation.

$$\gamma^{TB} = \gamma_F^{TB} + \gamma_P^{TB} \tag{4}$$

The average strain of material increases as more and more dislocations accumulate in the grains. These dislocations pile up against and/or travel across the TBs. Our atomistic simulations shown in Fig. 3 indicate that dislocations accumulate near the twin boundaries as the deformation proceeds. This process leads to rising strain gradients near the TBs, with strain increasing gradually from the crystal interior to the boundaries of the twin lamellae. The local mean strain gradient created by dislocations in the TBDPZ can be written as

$$\eta^{TB} = \frac{\gamma^{TB}}{d_{TBDPZ}} = \frac{\phi^{TB}(n_F^{TB} + n_P^{TB}/\sqrt{3})b}{d_{TBDPZ} d_G} \tag{5}$$

Here, d_{TBDPZ} denotes the thickness of TBDPZ and ϕ^{TB} is a geometric factor.

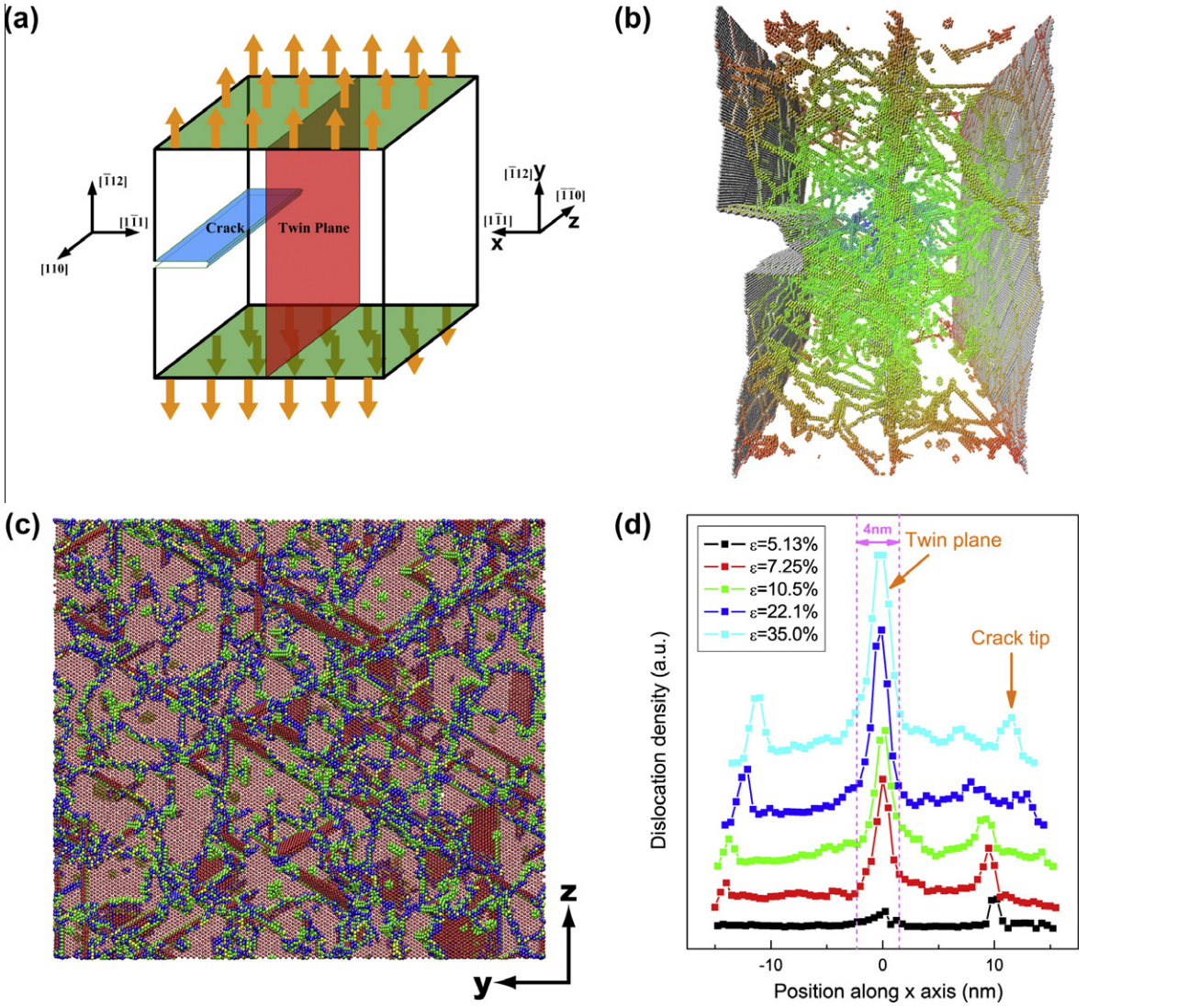

Fig. 3. Large-scale MD simulations of the TBDPZ through the interaction between a pre-existing TB and a large number of dislocations generated from a crack tip. (a) Schematic view of the simulation sample. (b) A snapshot of 3-D dislocation structures at a total strain of 22.1%, showing that the TB has become a wall of high dislocation density which can harden the material by blocking further dislocation activities; the gray atoms are on free surfaces, and other colors represent the distance of atoms near dislocation cores to the center of the simulated sample. (c) Patterns of dislocation structures remaining on the TB after a large number of dislocations have impinged and slipped across the twin plane; the coloring of atoms is based on the local crystalline order method. (d) Dislocation density distribution along the x-axis across the twin plane showing the characteristic thickness of the TBDPZ to be around 2.5–3.5 nm on each side of the TB. (For interpretation of the references to color in this figure legend, the reader is referred to the web version of this article.)

Note that the density of twinning partial dislocations in the twin lamella is defined as

$$\rho_{part} = \frac{n_P^{TB} \cdot L_0}{V} \tag{6}$$

where L_0 is the average length of the loop and V is the average volume of the twin lamellae. As twinning partials are stored along the TBs, their density in the twin lamellae can also be expressed as a function of the twin spacing as

$$\rho_{part} = \phi_p / d_{TB}^2 \tag{7}$$

Here, ϕ_p is a geometrical parameter and d_{TB} is the twin spacing. We can therefore express the number of twinning partials in the TBDPZ by combining Eqs. (6) and (7).

The density of inclined dislocations in the TBDPZ is defined as follows

$$\rho_{TB} = \chi \frac{n_F^{TB} \lambda^{TB}}{V_{Cell}} \tag{8}$$

where $\chi(=d_G/d_{TB})$ denotes the twin density in the grains and $V_{Cell}(=\pi d_G^3/6)$ is the volume of the unit cell; λ^{TB} is the average length of dislocation loops in the TBDPZ, which can be assumed to be d_G for simplicity. Consequently, combining Eq. (8) with Eq. (5), we can obtain the following expression for dislocation density in the TBDPZ,

$$\rho_{TB} = k^{TB} \frac{\tilde{\eta}^{TB}}{b} \tag{9}$$

Here, $k^{TB} = 12d_{TBDPZ}/\phi^{TB}\pi d_{TB}$, $\tilde{\eta}^{TB} = \eta^{TB} - \eta_P/d_{TB}$ and $\eta_P = \sqrt{3}\pi\phi_p b/12d_{TBDPZ}$. $\tilde{\eta}^{TB}$ denotes the effective local strain gradient in the TBDPZ. The second term of $\tilde{\eta}^{TB}$ is associated with the twinning partial dislocations, which can be ignored when the twin spacing is sufficiently large, resulting in $\tilde{\eta}^{TB} \approx \eta^{TB}$. Assuming that the maximum number of inclined dislocations in a grain is a constant N_0, their number in a unit twin lamella can be determined as $n_F^{TB} = N_0/\chi$. We then recast Eq. (5) as $\eta^{TB} = \eta_1 d_{TB} + \eta_0$ with $\eta_1 = \phi^{TB}N_0 b/(d_{TBDPZ}d_G^2)$ and $\eta_0 = \phi^{TB}n'_p b/(d_{TBDPZ}d_G\sqrt{3})$, n'_p being the number of initial twinning partials in the TBDPZ, which is independent of the twin spacing. The local strain gradient in the TBDPZ can be expressed as

$$\tilde{\eta}^{TB} = \eta_1 d_{TB} + \eta_0 - \eta_P/d_{TB} \tag{10}$$

Here, the parameters η_1, η_0 and η_P are all independent of the twin spacing and these parameters can be determined by fitting with experimental results.

3.1.2. Density of dislocations in GBDPZ

The GBDPZ refers to the region adjoining GBs that is actively involved in the plastic deformation through dislocation activities. We also assume that the plastic strain in the GBDPZ gradually increases from the grain interior to the GBs due to the individual slip steps moving away from the interface. The local strain gradient relevant to dislocations within the GB regions can be defined by

$$\eta^{GB} = \frac{\gamma^{GB}}{d_{GBDPZ}} \tag{11}$$

Here, d_{GBDPZ} denotes the thickness of GBDPZ and γ^{GB} is the plastic strain generated by dislocations in the GBDPZ, and can be expressed approximately as

$$\gamma^{GB} = \frac{\phi_3 n^{GB}\cdot b}{d_G} \tag{12}$$

where n^{GB} is the number of dislocations around the GBs and ϕ_3 is a geometrical factor. For simplicity, the average length λ^{GB} of dislocation loops in the GBDPZ can be assumed to be πd_G. Subsequently, the density of dislocations in the GBDPZ can be obtained as

$$\rho_{GB} = \frac{n^{GB}\lambda^{GB}}{V_{Cell}} = k^{GB}\frac{\eta^{GB}}{b} \tag{13}$$

where $k^{GB} = 6d_{GBDPZ}/\phi_3 d_G$.

3.1.3. Density of dislocations in crystal interior

For submicron grains, the intragrain dislocation-mediated interaction dominates the plastic deformation process. According to the Kocks–Mecking model, the density of dislocations in the crystal interior follows the following evolution law that accounts for the competition between accumulation and annihilation processes through dynamic recovery [32,33]:

$$\frac{\partial\rho_I}{\partial\varepsilon^{\mathrm{p}}} = M\left(\frac{k}{d_G} + k_1\sqrt{\rho_I} - k_2\rho_I\right) \tag{14}$$

where M is the Taylor factor, $k = 1/b; k_1 = \psi/b; k_2 = k_{20}(\dot{\varepsilon}^{\mathrm{p}}/\dot{\varepsilon}_0)^{-1/\mathrm{n}}$, ψ is a proportionality factor, k_{20} and $\dot{\varepsilon}_0$ are material constants, and n is inversely proportional to the temperature. The first and second terms on the right-hand side of the equation are associated with the athermal storage of dislocations and the third term is related to the annihilation of dislocations during dynamic recovery.

3.1.4. Effect of back stress on work hardening

Experiments have shown that work hardening becomes more pronounced with increasing twinning partial dislocations at sufficiently small twin spacing [10]. We assume that this phenomenon can be attributed to the fact that twinning partial dislocations move parallel to the TBs and can cross the whole grain before stopping at the GBs, accompanied by the migration of TBs during deformation [10,29]. Hence, the number of dislocations stopping at the GBs would increase with a reduction in twin spacing, as shown in Fig. 4. These dislocations give rise to a back stress that impedes the motion of other dislocations, leading to kinematic strain hardening [10,29]. Consequently, the back stress associated with twinning partial dislocations must be taken into account at small twin spacing. A common expression for such a back stress is

$$\sigma_b = M\frac{\mu b}{d_G}N \tag{15}$$

where N is the number of twinning partial dislocations stopping at the GBs, which depends on the plastic strain and can be calculated according to the following evolution law [23,34]:

$$\frac{dN}{d\varepsilon^p} = \frac{\zeta}{b}\left(1 - \frac{N}{N_B}\right) \tag{16}$$

Here, ε^p is the plastic strain, ζ is the mean spacing between slip bands and N_B is the maximum number of dislocation loops at the GBs.

3.2. Ductility of nanotwinned metal

Dislocations accumulated along the TBs are expected to facilitate a more uniform plastic deformation, which would in turn benefit the ductility of nanotwinned metals. With the high density of twinning partial dislocations at small twin spacing, the enhanced strain hardening further stabilizes plastic deformation against necking, leading to increased tensile ductility. Experimental observation [29] has also revealed that TBs can act as sources of dislocation nucleation. A simple fracture criterion based on soft mode activity has been proposed to correlate the failure strain to twin density within a two-dimensional model [20]. Additional failure mechanisms were considered by accounting for stress concentrations at triple junctions and GBs with the aid of a three-dimensional model for nanotwinned ultrafine crystals [21]. These studies suggest that there is competition between the different failure mechanisms when

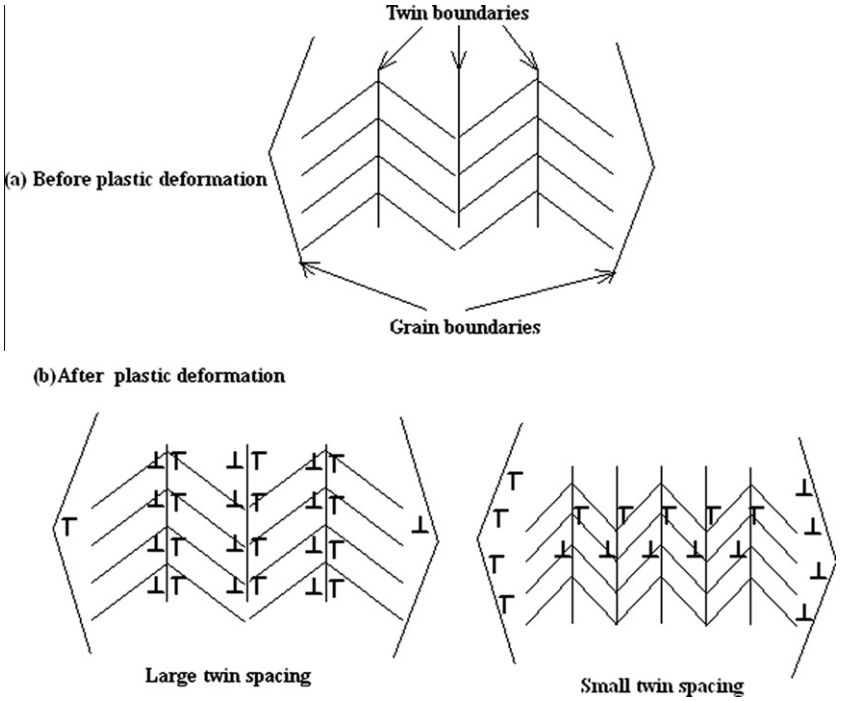

Fig. 4. Schematic drawings of dislocations piled up along the TBs and those that stop at the GBs. For a large twin spacing, a large number of dislocations are stored along the TBs and few dislocations stop at the GBs. In the case of a small twin spacing, the dislocations along the TBs vanish and the number of those that stop at the GBs increases, providing for the kinematic strain hardening in the nanotwinned metal.

twin spacing is reduced from 100 nm to just a few nanometers. In the following, the local flow stress in unit twin lamellae and GBs is calculated based on the Taylor model and compared with the stress required for nucleating dislocations, which will then be used as a new failure criterion for evaluating the ductility of nanotwinned metals.

3.2.1. Local flow stress in unit twin lamella and GBs

Experiments carried out on cracks in twinned metals have demonstrated that a crack tends to extend along the twin lamellae between two TBs [29,35]. Here a twin lamella is considered as a unit cell, as shown in Fig. 2a, and the local flow stress in the unit twin lamella is derived by taking into account contributions of dislocations in the TBDPZ and the crystal interior, as well as the effect of back stress.

Before analyzing the local flow stress from the Taylor relation, the density of dislocations in the TBDPZ of a unit twin lamella is recast as

$$\rho_{TB}^{unit} = \frac{n^{TB} \cdot d_G}{V_{unit}} \tag{17}$$

where $V_{unit} = \phi\pi d_G^2 d_{TB}/4$ is the average volume of the unit twin lamella and ϕ is a geometric factor; n^{TB} is the number of dislocations stored in the TBDPZ of the unit twin lamella. Note that the number of dislocations piled up along the boundaries and the applied shear stress τ_0 can be related as

$$n^{TB} = \frac{\tau_0 \pi L}{\mu b} \tag{18}$$

where L is the depth of dislocations piled up, which can be considered identical to the thickness d_{TBDPZ} of TBDPZ. Consequently, the local flow stress in the unit twin lamella can be expressed as

$$\tau_{flow} = \alpha\mu b\sqrt{\rho_I^{unit} + \rho_{TB}^{unit}} + \tau_b \tag{19}$$

where τ_b is the back stress and ρ_I^{unit} is the density of dislocations in the unit twin lamella, which can be determined from Eq. (14). For the local flow stress of GBs, there are plenty of dislocations stored in the GBDPZ, resulting in an expression similar to the local flow stress of the unit twin lamella, which is given as

$$\tau_{flow} = \alpha\mu b\sqrt{\rho_{GB}} + \tau_b \tag{20}$$

Here, ρ_{GB} is the density of dislocations in the GBDPZ, which can be determined from Eq. (13).

3.2.2. Critical stress for dislocation nucleation

The onset of fracture in materials often originates from the nucleation of dislocations. In describing cracks associated with dislocations, an opening crack can often be represented as a continuous array of dislocations [36]. As the crack grows, more dislocations will be nucleated at the front of the crack. During plastic deformation in nanotwinned copper, dislocations pile up along the TBs, leading to the nucleation of dislocations and eventual appearance of cracks in twin lamellae. Recent post-indentation studies of nanotwinned copper have indicated dislocation nucleation in the TBs [37]. The nucleation of perfect or partial dislocations has been investigated within the framework of a continuum model described by Asaro and Rice [38], a summary of which is presented below.

Consider the nucleation of a dislocation loop from a stress concentration as envisioned in Ref. [39]. The free energy of the expanding loop can be written as

$$U = \Phi r \ln(r/r_0) - \Re(r^{3/2} - r_0^{-3/2}) + \gamma \frac{1}{2}\pi(r^2 - r_0^2) \tag{21}$$

where γ represents the energy per unit area of the loop, which can be taken as the stacking fault energy, and

$$\Phi = \frac{\mu b_1^2(2-v)}{8(1-v)}, \Re = 1.4K_{II}b_1, K_{II} = \tau_{crit}\sqrt{\pi\frac{1}{2}d^*} \tag{22}$$

Here, b_1 is the magnitude of the Burgers vector. For a perfect dislocation b_1 equals b, whereas for a partial dislocation b_1 becomes $b/\sqrt{3}$; d^* equals d_{TB} for TBs and d_G for GBs. To determine the critical size of the loop and the critical value of the applied shear stress, we have the following two conditions [39]:

$$\frac{\partial U}{\partial r} = 0; \frac{\partial^2 U}{\partial r^2} = 0 \tag{23}$$

The critical stress for nucleation of a full or partial dislocation, τ_{crit}, can then be determined on the basis of the above equations.

To evaluate the ductility of nanotwinned metal, a new failure criterion is proposed:

$$\tau_{flow} \geqslant \tau_{crit} \tag{24}$$

This assumption implies that the unit twin lamella would start to fail as soon as the local flow stress exceeds the critical stress for spontaneous nucleation of dislocations in the lamellae. In nanotwinned copper with twin spacing less than 15 nm, the local stress in the unit twin lamella decreases with further reduced twin spacing, in which case the competition between different failure mechanisms at TBs and GBs must be taken into account. If the local flow stress in the GBs was greater than that in the TBs, the failure mechanism in the GBs would become dominant.

3.3. Mechanism-based gradient plasticity model for nanotwinned metals

The above equations have provided evolution laws of dislocation densities which are related to plastic strain gradient. Based on the strain gradient and Taylor model, a three dimensional stress–strain relation that incorporates the flow stress in Eq. (1) can be constructed from mechanism-based strain gradient plasticity [40–42]. Here we follow the conventional theory of mechanism-based strain gradient plasticity [42]. It should be noted that the stress–strain response of nanotwinned metals is strongly rate dependent, a phenomenon that has been studied in depth from a theoretical perspective [20,31]. However, in the present work we focus primarily on the effect of twin spacing on strengthening, ductility and work hardening. For convenience, the rate dependence is not rigorously considered in the present constitutive model. A brief summary of the adopted constitutive model is provided below.

The strain rate $\dot{\varepsilon}$ is decomposed into elastic and plastic parts,

$$\dot{\varepsilon} = \dot{\varepsilon}^{\mathbf{e}} + \dot{\varepsilon}^{\mathbf{p}} \tag{25}$$

The elastic strain rate follows the linear elastic relation

$$\dot{\varepsilon}^{\mathbf{e}} = \mathbf{M} : \dot{\sigma} \tag{26}$$

where $\mathbf{M}$ is the elastic compliance tensor, while the plastic strain rate is assumed to be proportional to the deviatoric stress $\boldsymbol{\sigma}'$ based on the J2-flow theory of plasticity, given as

$$\dot{\boldsymbol{\varepsilon}}^{\mathrm{p}} = \frac{3\dot{\varepsilon}^{\mathrm{p}}}{2\sigma_{\mathrm{e}}}\boldsymbol{\sigma}' \tag{27}$$

Here, $\sigma'_{ij} = \sigma_{ij} - \sigma_{kk}\delta_{ij}/3$ and $\sigma_e = \sqrt{3\sigma'_{ij}\sigma'_{ij}/2}$ is the von Mises stress; $\dot{\varepsilon}^{\mathrm{p}}$ is the equivalent plastic strain rate determined from

$$\dot{\varepsilon}^{\mathrm{p}} = \dot{\varepsilon}\left[\frac{\sigma_{\mathrm{e}}}{\sigma_{\mathrm{flow}}}\right]^{\mathrm{m}} \tag{28}$$

where $\dot{\varepsilon} = \sqrt{2\dot{\varepsilon}'_{ij}\dot{\varepsilon}'_{ij}/3}$ and $\dot{\varepsilon}'_{ij} = \dot{\varepsilon}_{ij} - \dot{\varepsilon}_{kk}\delta_{ij}/3$ is the deviatoric strain rate; m is a rate-sensitivity exponent, which must be sufficiently large to overcome the rate dependence [42]; σ_{flow} is the flow stress given in Eq. (1). Eqs. (26)–(28) then establish the three-dimensional (3-D) constitutive relation for a rate-independent, mechanism-based plasticity model for nanotwinned metals.

4. Numerical results and discussion

Nanotwinned copper is considered here as an example to validate the proposed model. The material parameters used for studying the deformation behavior of nanotwinned copper are listed in Table 1. These parameters were determined either directly from fitting experimental data [10] or extracted from the literature [43]. The local strain gradients in the TBDPZ and GBDPZ are treated as variables associated with the grain size and twin spacing, which can be determined by fitting experimental data. The two back stress parameters were determined from fitting with experimental results, which gave $\zeta = 25$ nm and $N_B = 10$.

4.1. Stress–strain curves

The true stress–strain curves predicted from the proposed constitutive model for nanotwinned copper with twin spacings of 4, 8, 10, 15, 35 and 96 nm are presented in Fig. 5 by adopting different local strain gradients in the TBDPZ, which are shown in the insets. Also included in these plots are the experimental results from Lu et al. [10]. Excellent agreement is shown in Fig. 5a between the model predictions and the experimental results for both yield stress and strain hardening. The proposed constitutive model appears to be capable of capturing the main features of the variation in yield stress with twin spacing changing between 15 and 96 nm. This agreement indicates

Table 1
Descriptions, symbols and magnitudes of different material parameters of the model.

Parameter (unit)	Symbol	Magnitude
Grain size (nm)	d_G	500
Elastic modulus (GPa)	E	128
Shear modulus (GPa)	μ	23.5
Poisson's ratio	v	0.36
Magnitude of the Burgers vector (nm)	b	0.256
Taylor factor	M	1.732∼3.06
Taylor constant	α	0.33
Thickness of GBDPZ (nm)	d_{GBDPZ}	3.6
Thickness of TBDPZ (nm)	d_{TBDPZ}	3.6
Mean spacing between slip bands (nm)	ζ	25
Maximum number of dislocation	N_B	10
Dynamic recovery constant	k_{20}	18.5
Proportionality factor	ψ	0.2
Dynamic recovery constant	n	12.5
Reference strain rate (s^{-1})	$\dot{\varepsilon}_0$	1
Stacking fault energy (meV $Å^{-2}$)	γ	2.260
Geometric factor	ϕ_p, ϕ^{TB}, $\phi_i (i = 1, 2, 3)$	0.5∼1.5

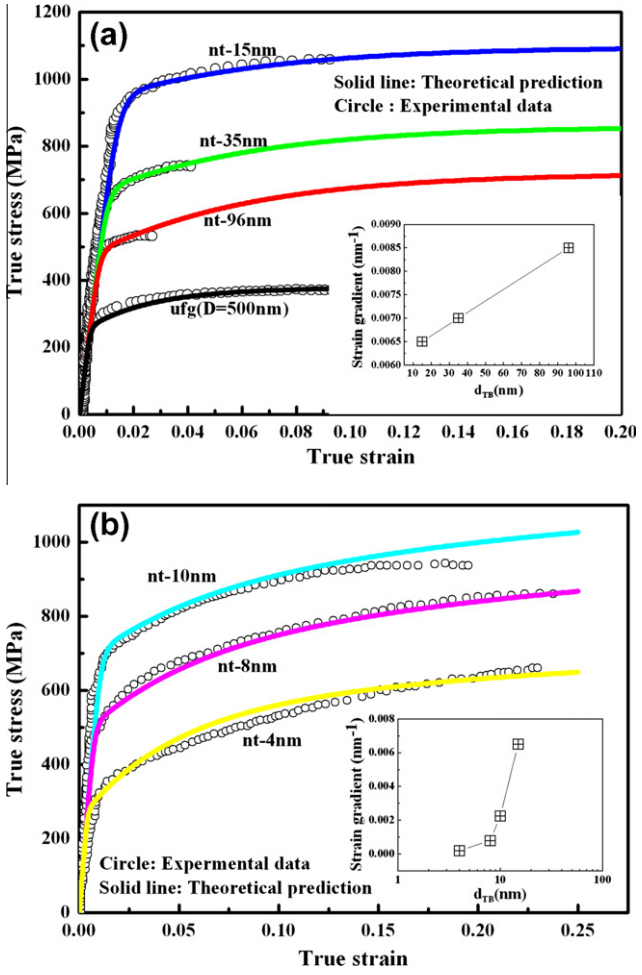

Fig. 5. (a) Simulated vs. experimental [10] tensile stress–strain responses of nanotwinned ultrafine-grained copper with twin spacings of 96, 35 and 15 nm and of ultrafine-grained copper free of twins. (b) Simulated vs. experimental [10] tensile stress–strain responses of nanotwinned ultrafine-grained copper with twin spacings of 10, 8 and 4 nm.

that the proposed model is sufficiently robust to predict the entire set of experimental results once the material parameters in the model are selected. The critical experimental observation of the softening of nanotwinned copper when the twin spacing falls below 15 nm has also been captured by the proposed model. Fig. 5b shows the predicted and experimentally measured true stress–true strain relationships of nanotwinned copper with twin spacings of 10, 8 and 4 nm, respectively. In these cases, the back stress plays an important role. Therefore, with the parameters shown in Table 1, the predicted yield stress and work hardening rate agree reasonably well with the experimental results for all the twin spacings under study. The insets in Fig. 5 show the variation in strain gradient with twin spacing. Note that the strain gradient drops sharply as the twin spacing falls below 15 nm. This is attributed to the emerging dominance of twinning partial dislocations below the critical twin spacing, which results in reduced dislocation pile-up along TBs and a rapid drop of strain gradient in the TBDPZs.

4.2. Onset of local fracture

Following the discussion in Section 3.2, a criterion for the onset of local fracture is invoked by comparing the local flow stress in the twin lamellae and GBs with the critical stress required for the homogeneous nucleation of dislocations. According to the proposed failure criterion, we plot the true stress–strain curves cut-off at the corresponding failure strains as the twin spacing is reduced from 96 to 4 nm, as shown in Fig. 6, where the local strain gradient in the TBDPZ given in Fig. 5 has been adopted. In comparison with the corresponding experimental results, the model results summarized in Fig. 6a show that for twin spacings larger than 15 nm the calculated failure strain agrees well with experimental values for twin spacing between 15 and 35 nm and slightly underestimates the experimental values for the twin spacing of 96 nm. For twin spacings less than 15 nm, the local flow stress is reduced due to the activity of twinning partial dislocations, and the onset of fracture changes from twin lamellae to GBs. The calculated failure

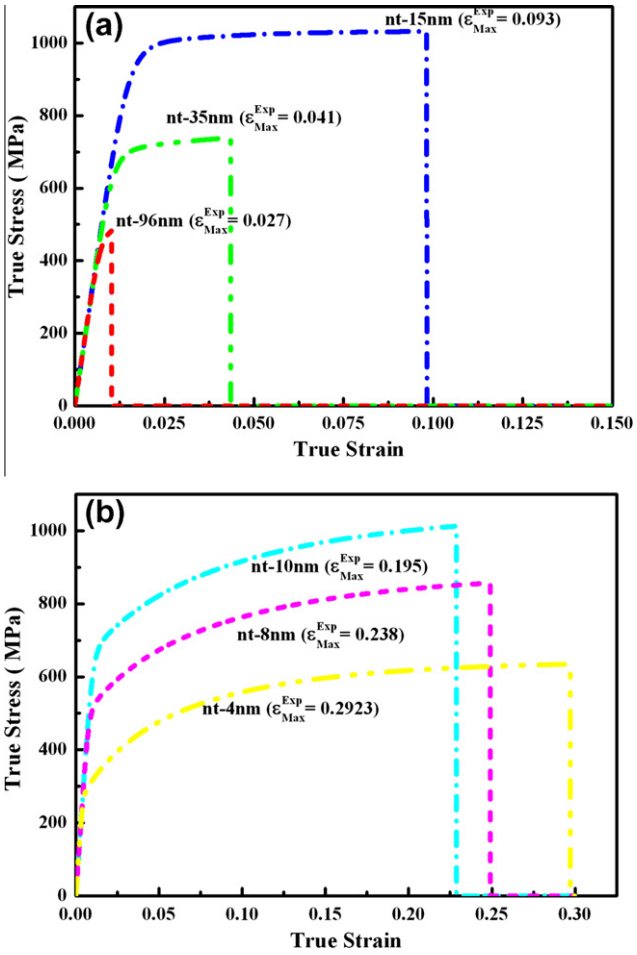

Fig. 6. Predictions for the ductility of nanotwinned copper with twin spacing ranging from 96 to 4 nm. The failure mechanism in the twin lamellae dominates the elongation process for large twin spacings (a) and the failure mechanism in the GBs becomes dominant over the failure mechanism in the twin lamellae for twin spacings less than 15 nm (b).

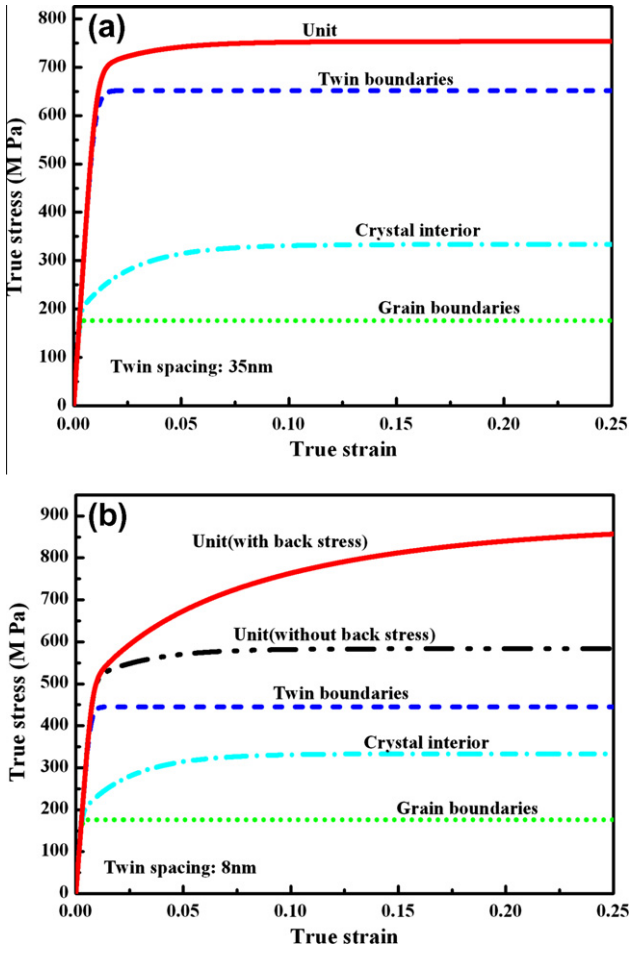

Fig. 7. The separate strengthening contributions associated with dislocations in the TBDPZ ($\sigma_{flow} = M\alpha\mu b\sqrt{\rho_{TB}}$), the GBDPZ ($\sigma_{flow} = M\alpha\mu b\sqrt{\rho_{GB}}$) and the crystal interior ($\sigma_{flow} = M\alpha\mu b\sqrt{\rho_1}$), and those associated with back stress for two selected cases in which twin spacing is taken as 35 nm and 8 nm.

strains at small twin spacings are shown in Fig. 6b. The predictions are in good agreement with the experimental results for twin spacing between 8 and 4 nm and slightly overestimate the twin spacing of 10 nm. Thus, our model has captured the variation in tensile ductility for all twin spacings under study.

4.3. Contributions from different deformation mechanisms

Fig. 7a and b compares contributions from different strengthening mechanisms in nanotwinned copper for twin spacings larger or smaller than the critical size of 15 nm. The most important terms are those representing the effect of back stress and contributions from dislocations in GBs, TBs and the crystal interior. For the case of 35 nm twin spacing, dislocations in the GBs and TBs are seen to mainly enhance the yield strength while dislocations in the crystal interior contribute to strain hardening. The contribution from dislocations in the TBs contributes the most to the enhancement of yield stress. In the case of 8 nm in twin spacing, dislocations in the TBs still make the largest contribution to the yield stress, while the effect of back stress on kinematic strain hardening is now much more prominent than that caused by dislocations in the crystal interior. The contributions from dislocations in the GBs and the crystal interior add to materials strengthening, similar to the 35 nm case. This can be attributed to the fact that the two samples have the same grain size.

Fig. 8 shows the stress–strain curves for twin spacings below 15 nm, where the effect of back stress is demonstrated by switching it on (solid curves) or off (dashed curves). An interesting finding is that the back stress only contributes to work hardening, with no tangible influence on yield stress. This may be explained by the fact that when the twin spacing is reduced to below the critical size, an increasing number of twinning partial dislocations participate in plastic deformation. These dislocations, once nucleated, can easily move across the whole grain before stopping at the GBs during deformation, leading to substantial back stress in dynamic strain hardening.

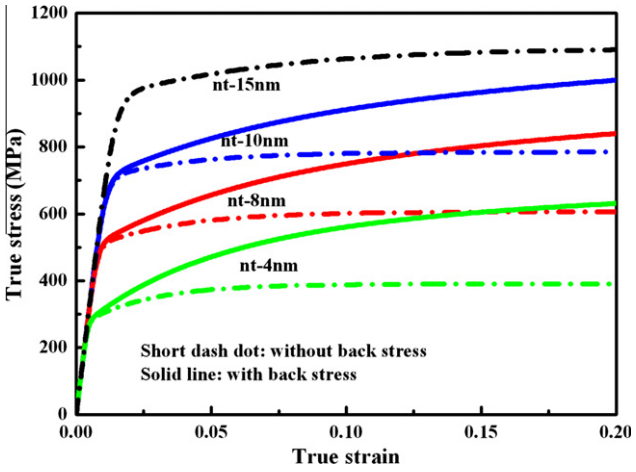

Fig. 8. Stress–strain curves for cases in which the effect of back stress on strain hardening is switched on (solid lines) or off (dashed lines) for twin spacings of 15, 10, 8 and 4 nm.

4.4. The critical twin spacing

The above discussions indicate that the local strain gradient in the TBDPZ contributes the most to the strengthening of nanotwinned copper. Fig. 9 shows the variations of strain gradient and dislocation density in the TBDPZ as the twin spacing is reduced from 96 to 4 nm. The data points pertaining to comparison with experiments were obtained from the fitting with experimental stress–strain curves shown in the insets of Fig. 5. Fitting Eq. (10) to these points leads to the solid line. These results demonstrate that the strain gradient increases rapidly for twin spacings smaller than 30 nm and then increases asymptotically towards a saturated value as the twin spacing increases to a large value. With the use of Eq. (9), the dislocation density in the TBDPZ is also plotted in Fig. 9. Note that the dislocation density peaks at a critical twin spacing around 13 nm and falls sharply as the twin spacing is further reduced. The maximum dislocation density, corresponding to the maximum yield stress, occurs at the critical twin spacing of 13 nm. This critical twin spacing agrees well with the experimentally measured value of 15 nm in nanotwinned copper [10].

Fig. 10a and b plots the variations in the yield stress and ductility as functions of twin spacing, with comparisons to the corresponding experimental results. Fig. 10a indicates that the yield stress increases as the twin spacing is reduced, until it reaches a maximum value at the critical twin spacing around 13 nm. Further reduction in twin spacing results in lower yield stress. Similar predictions have been made for the yield stress of nanocrystalline copper from MD simulations [44,45], although this phenomenon has not been confirmed by experiments in the absence of nanotwins. In contrast, our present predictions are in excellent agreement with the experimentally measured yield stress of nanotwinned copper for different twin spacings. Shown in Fig. 10b are two curves on the ductility vs. twin spacing of nanotwinned copper, predicted from two distinct failure criteria, i.e. failure from the GBs and failure from the twin lamellae. For large twin spacing, the failure tends to occur in the twin lamellae, with ductility increasing gradually as the twin spacing is reduced. Interestingly, the two failure curves intersect at the critical twin spacing of 13 nm, signifying a transition of the failure mechanism from failure in the twin lamellae to failure in the GBs. Fig. 10b shows that these predictions are in good agreement with the experimental observations [10]. Therefore, the present model seems capable of providing a unified quantitative description of strength and ductility of nanotwinned copper over a substantial range of transition across the critical twin spacing.

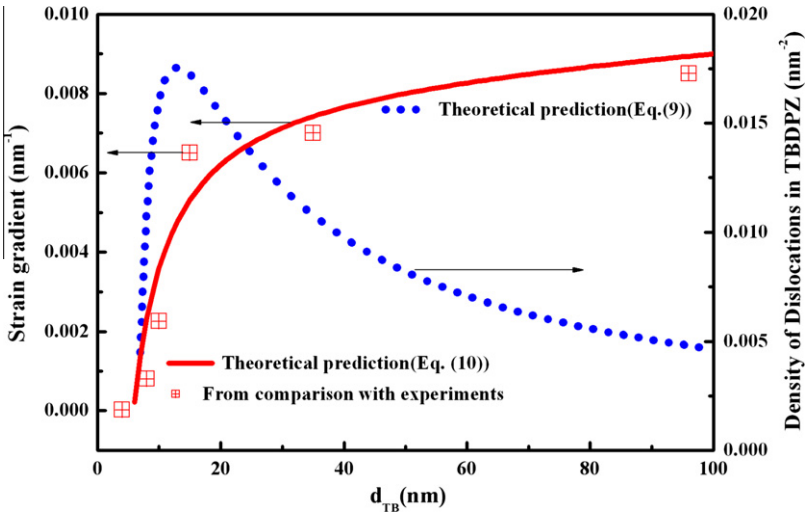

Fig. 9. The local strain gradient in the TBDPZ as a function of twin spacing obtained from the comparison between experiments and model predictions. Also shown in the plots are the corresponding fitting curves based on Eq. (10), and the curve of the dislocation density in the TBDPZ varied with twin spacing calculated from Eq. (9).

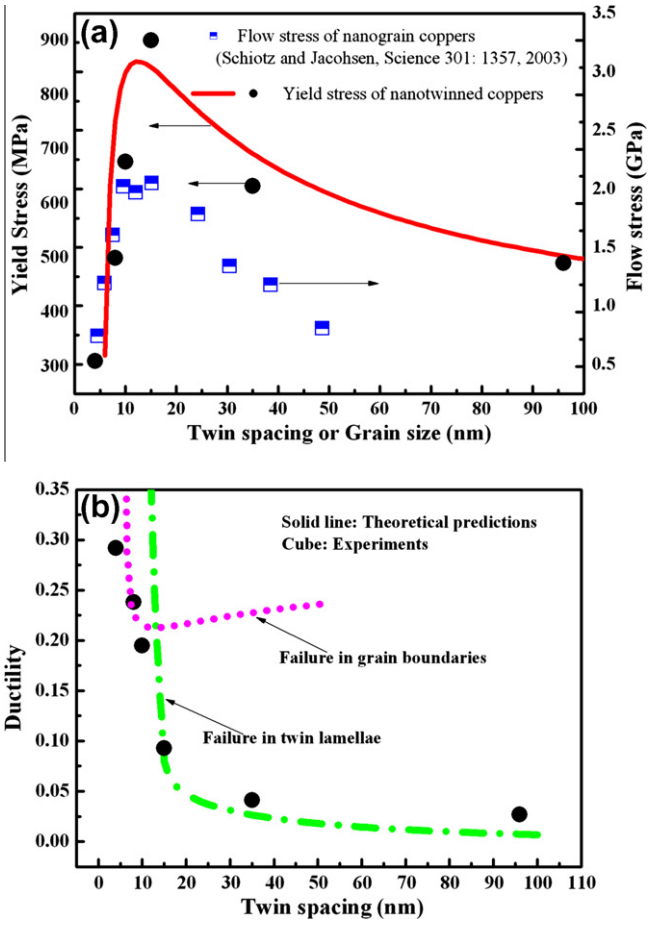

Fig. 10. The predicted yield stress (a) and ductility (b) of nanotwinned copper as functions of twin spacing in comparison with the corresponding experimental results. The lines are the predictions and the circles are the experimental data.

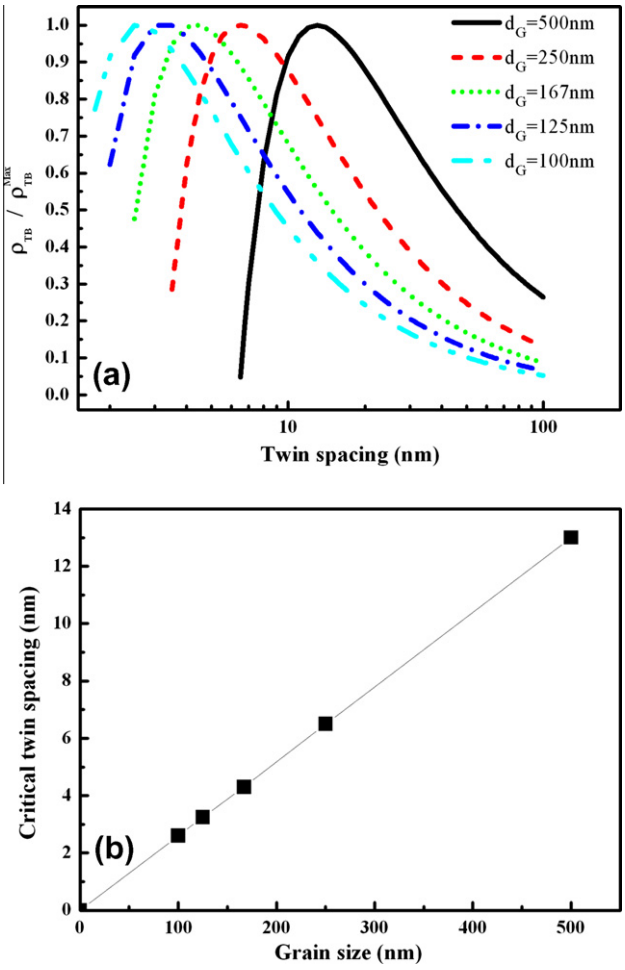

Fig. 11. (a) The density of dislocations in the TBDPZ as a function of twin spacing with different grain sizes; (b) the critical twin spacing as a function of grain size in the nanotwinned polycrystalline copper.

4.5. The effect of grain size

Another important issue is the relationship between the critical twin spacing and the grain size in a polycrystalline nanotwinned copper. Fig. 11a plots the density of dislocations in the TBDPZ vs. twin spacing with different grain sizes. These curves were normalized by the maximum density ρ_{TB}^{Max} for the corresponding grain size. It is clearly seen that the critical twin spacing decreases as the grain size is reduced from 500 to 100 nm. This result agrees well with recent MD simulations of strengthening in nanotwinned copper [28]. To determine the exact relation between the critical twin spacing and grain size, we differentiate Eq. (9) with respect to the twin spacing and obtain a critical value $d_{TB}^{tra} = \eta_0/2\eta_p$, which is related to the grain size in Fig. 11b. It is noted that the critical twin spacing is a linear function of grain size, in agreement with the MD simulations and the prediction from a dislocation nucleation model [28]. The effect of grain size on the critical twin spacing provides another possible route for the optimized design of high-strength, high-ductility metals.

4.6. Comparison with MD simulations

The model proposed in this work has been used to capture the variations in strength, work hardening and tensile ductility of nanotwinned copper with twin spacing ranging from 100 to 4 nm. In particular, the model has considered the contribution of twinning partial dislocations to plastic deformation, which is the main cause for the reduction in yield strength at small twin spacing, as shown by MD simulations [28]. Since the present study mainly focuses on the effect of twin spacing on yield strength, strain hardening and tensile ductility, the strain-rate effect has not been rigorously considered. In the analysis we have used comparisons between experimental stress–strain curves and corresponding numerical calculations to determine the strain gradient in the TBDPZ, which is further related to the twin spacing by Eq. (10). As the twin spacing is reduced to below the critical size, the activity of twinning partial dislocations makes the last term on the right-hand side of Eq. (10) predominant, leading to substantial reduction in yield strength. This is consistent with the results of MD simulations, which demonstrated that the activities of

twinning partial dislocations dominate the softening behavior in nanotwinned copper when the twin spacing falls below the critical value [28]. In addition to the effect of twin spacing, the present model also shows that the critical twin spacing scales linearly with the grain size, which is in perfect agreement with the MD simulation results and the predicted behavior from a twinning partial dislocation nucleation model [28]. In comparison with MD simulations, an important benefit of the present model, which builds upon the continuum theory of mechanism-based strain gradient plasticity, is that the grain size of nanotwinned metal can be varied from the nanometer scale to the micrometer or even larger scale. This would have been very challenging for MD simulations.

5. Conclusions

The present work has developed a dislocation density-based physical model generalizing the mechanism-based strain gradient plasticity [40–42] for the constitutive description of nanotwinned metals. The work is aimed at providing a quantitative description of the effect of twin spacing and grain size on the flow stress, strain hardening and ductility of nanotwinned metals. The concept of dislocation pile-up zones near TBs and GBs, which lead to substantial strain gradients in such zones, is adopted in the proposed model. Large-scale MD simulations have been performed to validate the critical assumption of the existence of TBDPZ and to determine its thickness. The contributions of twinning partial dislocations to the deformation of nanotwinned metals are taken into account in the model, which enabled a quantitative description of the strengthening and hardening transition across a critical twin spacing for the maximum flow stress. In addition, a local fracture criterion has been employed to estimate the tensile ductility of nanotwinned metals. After the model parameters are identified from experiments, the proposed constitutive model shows reasonable quantitative agreements with a broad range of experimental results on strength, strain hardening and ductility of nanotwinned copper. Combined with experimental and atomistic simulation studies in the literature, our study demonstrates that the correlated properties of high strength, high ductility and strong work hardening in nanotwinned metals are sensitive to both twin spacing and grain size. The results reported in this paper show that the proposed theoretical model can be used as an efficient tool to enhance and balance strength, ductility and work hardening in nanotwinned polycrystals through the optimal design of twin lamellae and grains microstructures.

Acknowledgements

L.Z., H.R. and J.L. gratefully acknowledge the support from the Research Grants Council of the Hong Kong Special Administrative Region of China under grants CityU8/CRF/08 and GRF/CityU519110, the Croucher Fundation CityU9500006, and the PolyU Postdoctoral Fellowship project (G-YX3S). M.D. further acknowledges the financial support by the ONR Grant N00014-08-1-0510, and by the Advanced Materials for Micro and Nano Systems Program of the Singapore-MIT Alliance (SMA). X.L. and H.G. acknowledge financial support by NSF through the MRSEC Program (award number DMR-0520651) and grant CMMI-0758535 at Brown University. The atomistic simulations reported were performed on NSF TeraGrid resources provided by NICS under MSS090046 (H.G.), with additional support from the Computational Mechanics Research Facility at Brown University.

References

[1] Lu K, Lu L, Suresh S. Science 2009;324:349–52.
[2] Lu L, Shen YF, Chen XH, Qian LH, Lu K. Science 2004;304:422–6.
[3] Dao M, Lu L, Asaro RJ, De Hosson JTM, Ma E. Acta Mater 2007;55:4041–65.
[4] Wang YM, Chen MW, Zhou FH, Ma E. Nature 2002;419:912–5.
[5] Zhao YH, Topping T, Bingert JF, Dangelewicz AM, Li Y, Zhu YT, et al. Adv Mater 2008;20:3028–33.
[6] Fan JT, Chen AY, Fu MW, Lu J. Scripta Mater 2009;61:608–11.
[7] Chen AY, Li DF, Zhang JB, Song HW, Lu J. Scripta Mater 2008;59:579–82.
[8] Zhang X, Misra, Wang H, Shen TD, Nasasi M, Mitchell TE, et al. Acta Mater 2004;52:995–1002.
[9] Shen YF, Lu L, Dao M, Suresh S. Scripta Mater 2006;55:319–22.
[10] Lu L, Chen X, Huang X, Lu K. Science 2009;323:607–10.
[11] Jin ZH, Gumbsch P, Ma E, Albe K, Lu K, Hahn H, et al. Scripta Mater 2006;54:1163–8.
[12] Jin ZH, Gumbsch P, Albe K, Ma E, Lu K, Gleiter H, et al. Acta Mater 2008;56:1126–35.
[13] Cao AJ, Wei YG, Mao SX. Appl Phys Lett 2007;90(1-3):151909.
[14] Froseth A, Van Swygenhoven H, Derlet PM. Acta Mater 2004;52:4041–65.
[15] Froseth A, Derlet PM, Van Swygenhoven H. Appl Phys Lett 2004;85:5863–5.
[16] Afanasyev KA, Sansoz F. Nano Lett 2007;7:2056–62.
[17] Zheng YG, Lu J, Zhang HW, Chen Z. Scripta Mater 2009;60:508–11.
[18] Cao AJ, Wei YG. J Appl Phys 2007;102(1-5):83511.
[19] Zhu T, Li J, Samanta A, Kim HG, Suresh S. Proc Natl Acad Sci 2007;104:3031–6.
[20] Dao M, Lu L, Shen Y, Suresh S. Acta Mater 2006;54:5421–32.
[21] Jerusalem A, Dao M, Suresh S, Radovitzky R. Acta Mater 2008;56:4647–57.
[22] Allain S, Chateau JP, Bouaziz O. Mater Sci Eng A 2004;387–389:143–7.
[23] Bouaziz O, Allain S, Scott C. Scripta Mater 2008;58:484–7.
[24] Gil Sevillano J. Scripta Mater 2009;60:336–9.
[25] Schwaiger R, Moser B, Dao M, Chollacoop N, Suresh S. Acta Mater 2003;51:5159–72.
[26] Lu L, Schwaiger R, Shan ZW, Dao M, Lu K, Suresh S. Acta Mater 2005;53:2169–79.
[27] Shen YF, Lu L, Lu QH, Jin ZH, Lu K. Scripta Mater 2005;52:989–94.
[28] Li XY, Wei YJ, Lu L, Lu K, Gao HJ. Nature 2010;464:877–80.
[29] Shan ZW, Lu L, Minor AM, Stach EA, Mao SX. JOM 2008;60:71–4.
[30] Kim S-W, Li XY, Gao HJ, Kumar, KS. Submitted for publication.
[31] Lu L, Zhu T, Shen Y, Dao M, Lu K, Suresh S. Acta Mater 2009;57:5165–73.
[32] Kocks UF, Mecking H. Prog Mater Sci 2003;48:171–273.
[33] Capolungo L, Jochum C, Cherkaoui M, Qu J. Int J Plasticity 2005;21:67–82.
[34] Sinclair CW, Poole WJ, Bréchet Y. Scripta Mater 2006;55:739–42.

[35] Qu S, Zhang P, Wu SD, Zang QS, Zhang ZF. Scripta Mater 2008;59:1131–4.
[36] Bilay BA, Eshelby JD. In: Liebowitz H, editor. Fracture, vol. 1. New York: Academic Press; 1969. p. 99–182.
[37] Kumar KS, Suresh S, Chisholm MF, Horton JA, Wang P. Acta Mater 2003;51:387–405.
[38] Asaro RJ, Rice JR. J Mech Phys Solids 1977;25:309–38.
[39] Asaro RJ, Suresh S. Acta Mater 2005;53:3369–82.
[40] Nix WD, Gao H. J Mech Phys Solids 1998;46:411–25.
[41] Gao HJ, Huang YG, Nix WD, Hutchinson JW. J Mech Phys Solids 1999;47:1239–63.
[42] Huang Y, Qu S, Hwang KC, Li M, Gao H. Int J Plasticity 2004;20:753–82.
[43] Kim HS, Estrin Y, Bush MB. Acta Mater 2000;48:493–504.
[44] Schiotz J, Jacobsen KW. Science 2003;301:1357–9.
[45] Yip S. Nature 1998;391:532–3.